
RenderNet: A deep convolutional network for differentiable rendering from 3D shapes

Thu Nguyen-Phuoc
University of Bath
T.Nguyen.Phuoc@bath.ac.uk

Chuan Li
Lambda Labs
c@lambdalabs.com

Stephen Balaban
Lambda Labs
s@lambdalabs.com

Yong-Liang Yang
University of Bath
Y.Yang@cs.bath.ac.uk

Abstract

Traditional computer graphics rendering pipelines are designed for procedurally generating 2D images from 3D shapes with high performance. The non-differentiability due to discrete operations (such as visibility computation) makes it hard to explicitly correlate rendering parameters and the resulting image, posing a significant challenge for inverse rendering tasks. Recent work on differentiable rendering achieves differentiability either by designing surrogate gradients for non-differentiable operations or via an approximate but differentiable renderer. These methods, however, are still limited when it comes to handling occlusion, and restricted to particular rendering effects. We present RenderNet, a differentiable rendering convolutional network with a novel projection unit that can render 2D images from 3D shapes. Spatial occlusion and shading calculation are automatically encoded in the network. Our experiments show that RenderNet can successfully learn to implement different shaders, and can be used in inverse rendering tasks to estimate shape, pose, lighting and texture from a single image.

1 Introduction

Rendering refers to the process of forming a realistic or stylized image from a description of the 3D virtual object (e.g., shape, pose, material, texture), and the illumination condition of the surrounding scene (e.g., light position, distribution, intensity). On the other hand, inverse rendering (graphics) aims at estimating these properties from a single image. The two most popular rendering methods, rasterization-based rendering and ray tracing, are designed to achieve fast performance and realism respectively, but not for inverse graphics. These two methods rely on discrete operations, such as z-buffering and ray-object intersection, to identify point visibility in a rendering scene, which makes these techniques non-differentiable. Although it is possible to treat them as non-differentiable renderers in computer vision tasks [1], inferring parameters, such as shapes or poses, from the rendered images using traditional graphics pipelines is still a challenging task. A differentiable renderer that can correlate the change in a rendered image with the change in rendering parameters therefore will facilitate a range of applications, such as vision-as-inverse-graphics tasks or image-based 3D modelling and editing.

Recent work in differentiable rendering achieves differentiability in various ways. Loper and Black [2] propose an approximate renderer which is differentiable. Kato et al. [3] achieve differentiability by proposing an approximate gradient for the rasterization operation. Recent work on image-based reconstruction uses differentiable projections of 3D objects onto silhouette masks as a surrogate for a rendered image of the objects [4, 5]. Wu et al. [6] and Tulsiani et al. [7] derive differentiable projective

functions from normal, depth, and silhouette maps, but respectively can only handle orthographic projection, or needs multiple input images. These projections can then be used to construct an error signal for the reconstruction process. All of these approaches, however, are restricted to specific rendering styles (rasterization) [2, 3, 8], input geometry types [9, 10], or limiting output formats such as depth or silhouette maps [4, 5, 6, 7, 11, 12]. Moreover, none of these approaches try to solve the problem from the network architecture design point of view. Recent progress in machine learning shows that network architecture plays an important role for improving the performance of many tasks. For example, in classification, ResNet [13] and DenseNet [14] have contributed significant performance gains. In segmentation tasks, U-Net [15] proves that having short-cut connections can greatly improve the detail level of the segmentation masks. In this paper, we therefore focus on designing a neural network architecture suitable for the task of rendering and inverse rendering.

We propose RenderNet, a convolutional neural network (CNN) architecture that can be trained end-to-end for rendering 3D objects, including object visibility computation and pixel color calculation (shading). Our method explores the novel idea of combining the ability of CNNs with inductive biases about the 3D world for geometry-based image synthesis. This is different from recent image-generating CNNs driven by object attributes [16], noise [17], semantic maps [18], or pixel attributes [19], which make very few assumption about the 3D world and the image formation process. Inspired by the literature from computer graphics, we propose the projection unit that incorporates prior knowledge about the 3D world, and how it is rendered, into RenderNet. The projection unit, through learning, is a differentiable approximation of the non-differentiable visibility computation step, making RenderNet an end-to-end system. Unlike non-learned approaches in previous work, a learned projection unit uses deep features instead of low-level primitives, making RenderNet generalize well to a variety of input geometries, robust to erroneous or low-resolution input, as well as enabling learning multi-style rendering with the same network architecture. RenderNet is differentiable and can be easily integrated to other neural networks, benefiting various inverse rendering tasks, such as novel-view synthesis, pose prediction, or image-based 3D shape reconstruction, unlike previous image-based inverse rendering work that can recover only part of the full 3D shapes [20, 21].

We choose the voxel presentation of 3D shapes for its regularity and flexibility, and its application in visualizing volumetric data such as medical images. Although voxel grids are traditionally memory inefficient, computers are becoming more powerful, and recent work also addresses this inefficiency using octrees [22, 23], enabling high-resolution voxel grids. In this paper, we focus on voxel data, and leave other data formats such as polygon meshes and unstructured point clouds as possible future extensions. We demonstrate that RenderNet can generate renderings of high quality, even from low-resolution and noisy voxel grids. This is a significant advantage compared to mesh renderers, including more recent work in differentiable rendering, which do not handle erroneous inputs well.

By framing the rendering process as a feed-forward CNN, RenderNet has the ability to learn to express different shaders with the same network architecture. We demonstrate a number of rendering styles ranging from simple shaders such as Phong shading [24], suggestive contour shading [25], to more complex shaders such as a composite of contour shading and cartoon shading [26] or ambient occlusion [27], some of which are time-consuming and computationally expensive. RenderNet also has the potential to be combined with neural style transfer to improve the synthesized results, or other complex shaders that are hard to define explicitly.

In summary, the proposed RenderNet can benefit both rendering and inverse rendering: RenderNet can learn to generate images with different appearance, and can also be used for vision-as-inverse-graphics tasks. Our main contributions are threefold.

- A novel convolutional neural network architecture that learns to render in different styles from a 3D voxel grid input. To our knowledge, we are the first to propose a neural renderer for 3D shapes with the projection unit that enables both rendering and inverse rendering.
- We show that RenderNet generalizes well to objects of unseen category and more complex scene geometry. RenderNet can also produce textured images from textured voxel grids, where the input textures can be RGB colors or deep features computed from semantic inputs.
- We show that our model can be integrated into other modules for applications, such as texturing or image-based reconstruction.

2 Related work

Our work is related to three categories of learning-based works: image-based rendering, geometry-based rendering and image-based shape reconstruction. In this section, we review some landmark methods that are closely related to our work. In particular, we focus on neural-network-based methods.

Image-based rendering There is a rich literature of CNN-based rendering by learning from images. Dosovitskiy et al. [16] create 2D images from low-dimensional vectors and attributes of 3D objects. Cascaded refinement networks [18], and Pix2Pix [28] additionally condition on semantic maps or sketches as inputs. Using a model that is more deeply grounded in computer graphics, DeepShading [19] learns to create images with high fidelity and complex visual effects from per-pixel attributes. DC-IGN [29] learns disentangled representation of images with respect to transformations, such as out-of-plane rotations and lighting variations, and thus is able to edit images with respect to these factors. Relevant works on novel 3D view synthesis [30] leverage category-specific shape priors and optical flow to deal with occlusion/disocclusion. While these methods yield impressive results, we argue that geometry-based methods, which make stronger assumptions about the 3D world and how it produces 2D images, will be able to perform better in certain tasks, such as out-of-plane rotation, image relighting, and shape texturing. This also coincides with Rematas et al. [31], Yang et al. [32] and Su et al. [33] who use strong 3D priors to assist the novel-view synthesis task.

Geometry-based rendering Despite the rich literature in rendering in computer graphics, there is a lot less work using differentiable rendering techniques. OpenDR [2] has been a popular framework for differentiable rendering. However, being a more general method, it is more strenuous to be integrated into other neural networks and machine learning frameworks. Kato et al. [3] approximate the gradient of the rasterization operation to make the rendering differentiable. However, this method is limited to rasterization-based rendering, making it difficult to represent more complex effects that are usually achieved by ray tracing such as global illumination, reflection, or refraction.

Image-based 3D shape reconstruction Reconstructing 3D shape from 2D image can be treated as estimating the posterior of the 3D shape conditioned on the 2D information. The prior of the shape could be a simple smoothness prior or a prior learned from 3D shape datasets. The likelihood term, on the other hand, requires estimating the distribution of 2D images given the 3D shape. Recent work has been using 2D silhouette maps of the images [4, 5]. While this proves effective, silhouette images contain little information about the shape. Hence a large number of images or views of the object is required for the reconstruction task. For normal maps and depth maps of the shape, Wu et al. [6] derive differentiable projective functions assuming orthographic projection. Similarly, Tulsiani et al. [7] propose a differentiable formulation that enables computing gradients of the 3D shape given multiple observations of depth, normal or pixel color maps from arbitrary views. In our work, we propose RenderNet as a powerful model for the likelihood term. To reconstruct 3D shapes from 2D images, we do MAP estimation using our trained rendering network as the likelihood function, in addition to a shape prior that is learned from a 3D shape dataset. We show that we can recover not only the pose and shape, but also lighting and texture from a single image.

3 Model

The traditional computer graphics pipeline renders images from the viewpoint of a virtual pin-hole camera using a common perspective projection. The viewing direction is assumed to be along the negative z-axis in the camera coordinate system. Therefore, the 3D content defined in the world coordinate system needs to be transformed into the camera coordinate system before being rendered. The two currently popular rendering methods, rasterization-based rendering and ray tracing, procedurally compute the color of each pixel in the image with two major steps: testing visibility in the scene, and computing shaded color value under an illumination model.

RenderNet jointly learns both steps of the rendering process from training data, which can be generated using either rasterization or ray tracing. Inspired by the traditional rendering pipeline, we also adopt the world-space-to-camera-space coordinate transformation strategy, and assume that the camera is axis-aligned and looks along the negative z-axis of the volumetric grid that discretizes the input shape. Instead of having the network learn operations which are differentiable and easy to implement, such as rigid-body coordinate transformation or the interaction of light with surface

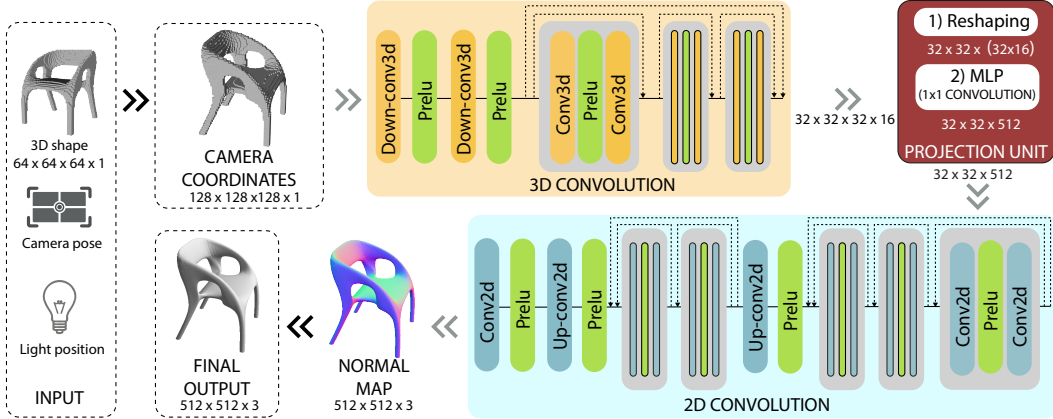


Figure 1: **Network architecture.** See Section 2 in the supplementary document for details.

normals (e.g. assuming a Phong illumination model [24]), we provide most of them explicitly to the network. This allows RenderNet to focus its capacity on more complex aspects of the rendering task, such as recognizing visibility and producing shaded color.

RenderNet receives a voxel grid as input, and applies a rigid-body transformation to convert from the world coordinate system to the camera coordinate system. The transformed input, after being trilinearly sampled, is then fed to a CNN with a projection unit to produce a rendered 2D image. RenderNet consists of 3D convolutions, a projection unit that computes visibility of objects in the scene and projects them onto 2D feature maps, followed by 2D convolutions to compute shading.

We train RenderNet using a pixel-space loss between the target image and the output. Optionally, the network can produce normal maps of the 3D input which can be combined with light sources to illuminate the scene. While the projection unit can easily incorporate orthographic projections, the 3D convolutions can morph the scene and allows for perspective camera views. In future versions of RenderNet, perspective transformation may also be explicitly incorporated into the network.

3.1 Rotation and resampling

The transformed input via rigid body motion ensures that the camera is always in the same canonical pose relative to the voxel grid being rendered. The transformation is parameterized by the rotation around the y-axis and z-axis, which corresponds to the azimuth and elevation, and a distance R that determines the scaling factor, i.e., how close the object is to the camera. We embedded the input voxel grid into a larger grid to make sure the object is not cut off after rotation. The total transformation therefore includes scaling, rotation, translation, and trilinear resampling.

3.2 Projection unit

The input of RenderNet is a voxel grid V of dimension $H_V \times W_V \times D_V \times C_V$ (corresponding to height, width, depth, and channel), and the output is an image I of dimension $H_I \times W_I \times C_I$ (corresponding to height, width and channel). To bridge the disparity between the 3D input and 2D output, we devise a novel projection unit. The design of this unit is straightforward: it consists of a reshaping layer, and a multilayer perceptron (MLP). Max pooling is often used to flatten the 3D input across the depth dimension [4, 5], but this can only create the silhouette map of the 3D shape. The projection unit, on the other hand, learns not only to perform projection, but also to determine visibility of different parts of the 3D input along the depth dimension after projection.

For the reshaping step of the unit, we collapse the depth dimension with the feature maps to map the incoming 4D tensor to a 3D squeezed tensor V' with dimension $W \times H \times (D \cdot C)$. This is immediately followed by an MLP, which is capable of learning more complex structure within the local receptive field than a conventional linear filter [13]. We apply the MLP on each $(D \cdot C)$ vector, which we implement using a 1×1 convolution in this project. The reshaping step allows each unit of the MLP to access the features across different channels and the depth dimension of the input, enabling the

network to learn the projection operation and visibility computation along the depth axis. Given the squeezed 3D tensor V' with $(D \cdot C)$ channels, the projection unit produces a 3D tensor with K channels as follows:

$$I_{i,j,k} = f \left(\sum_{dc} w_{k,dc} \cdot V'_{i,j,dc} + b_k \right) \quad (1)$$

where i, j are pixel coordinates, k is the image channel, dc is the squeezed depth channel, where d and c are the depth and channel dimension of the original 4D tensor respectively, and f is some non-linear function (parametric ReLU in our experiments).

3.3 Extending RenderNet

We can combine RenderNet with other networks to handle more rendering parameters and perform more complex tasks such as shadow rendering or texture mapping. We model a conditional renderer $p(I | V, h)$ where h can be extra rendering parameter such as lights, or spatially-varying parameters such as texture.

Here we demonstrate the extensibility of RenderNet using the example of the Phong illumination model [24]. The per-pixel shaded color for the images is calculated by $S = \max(0, \vec{l} \cdot \vec{n} + a)$, where \vec{l} is the unit light direction vector, \vec{n} is the normal vector, whose components are encoded by the RGB channels of the normal map, and a is an ambient constant. Shading S and albedo map A are further combined to create the final image I based on $I = A \odot S$ [34]. This is illustrated in Section 4.1, where we combine the albedo map and normal map rendered by the combination of a texture-mapping network and RenderNet to render shaded images of faces.

4 Experiments

To explore the generality of RenderNet, we test our method on both computer graphics and vision tasks. First, we experiment with different rendering tasks with varying degree of complexity, including challenging cases such as texture mapping and surface relighting. Second, we experiment with vision applications such as image-based pose and shape reconstruction.

Datasets We use the chair dataset from ShapeNet Core [35]. Apart from being one of the categories with the largest number of data points (6778 objects), the chair category also has large intra-class variation. We convert the ShapeNet Dataset to $64 \times 64 \times 64$ voxel grids using volumetric convolution [36]. We randomly sampled 120 views of each object to render training images at 512×512 resolution. The elevation and azimuth are uniformly sampled between $[10, 170]$ degrees and $[0, 359]$ degrees, respectively. Camera radius are set at 3 to 6.3 units from the origin, with the object’s axis-aligned bounding box normalized to 1 unit length. For the texture mapping tasks, we generate 100,000 faces from the Basel Face Dataset [37], and render them with different azimuths between $[220, 320]$ degrees and elevations between $[70, 110]$ degrees. We use Blender3D to generate the Ambient Occlusion (AO) dataset, and VTK for the other datasets. For the contour dataset, we implemented the pixel-based suggestive contour [25] algorithm in VTK.

Training We adopt the patch training strategy to speed up the training process in our model. We train the network using random spatially cropped samples (along the width and height dimensions) from the training voxel grids, while keeping the depth and channel dimensions intact. We only use the full-sized voxel grid input during inference. The patch size starts as small as 1/8 of the full-sized grid, and progressively increases towards 1/2 of the full-sized grid at the end of the training.

We train RenderNet using a pixel-space regression loss. We use mean squared error loss for colored images, and binary cross entropy for grayscale images. We use the Adam optimizer [38], with a learning rate of 0.00001.

Code, data and trained models will be available at: <https://github.com/thunguyenphuoc/RenderNet>.

4.1 Learning to render and apply texture

Figure 2 shows that RenderNet is able to learn different types of shaders, including Phong shading, contour line shading, complex multi-pass shading (cartoon shading), and a ray-tracing effect (Ambient

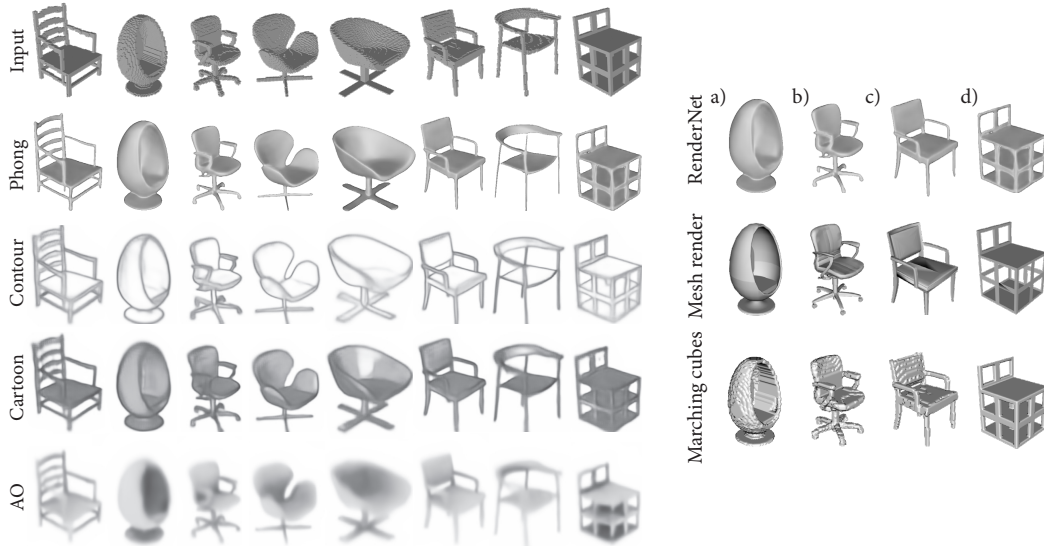


Figure 2: **Left:** Different types of shaders generated by RenderNet (input at the top). **Right:** Comparing Phong shading between RenderNet, a standard OpenGL mesh renderer, and a standard Marching Cubes algorithm. RenderNet produces competitive results with the OpenGL mesh renderer without suffering from mesh artefacts (notice the seating pad of chair (c) or the leg of chair (d) in Mesh renderer), and does not suffer from low-resolution input like Marching cubes.

Occlusion) with the same network architecture. RenderNet was trained on datasets for each of these shaders, and the figure shows outputs generated for unseen test 3D shapes. We report the PSNR score for each shader in Figure 5.

RenderNet generalizes well to shapes of unseen categories. While it was trained on chairs, it can also render non-man-made objects such as the Stanford Bunny and Monkey (Figure 3). The method also works very well when there are multiple objects in the scene, suggesting the network recognizes the visibility of the objects in the scene.

RenderNet can also handle corrupted or low-resolution volumetric data. For example, Figure 3 shows that the network is able to produce plausible renderings for the Bunny when the input model was artificially corrupted by adding 50% random noise. When the input model is downsampled (here we linearly downsampled the input by 50%), RenderNet can still render a high-resolution image with smooth details. This is advantageous compared to the traditional computer graphics mesh rendering, which requires a clean and high-quality mesh in order to achieve good rendered results.

It is also straightforward to combine RenderNet with other modules for tasks such as mapping and rendering texture (Figure 4). We create a texture-mapping network to map a 1D texture vector representation (these are the PCA coefficients for generating albedo texture using the BaseFace dataset) to a 3D representation of the texture that has the same width, height and depth as the shape input. This output is concatenated along the channel dimension with the input 3D shape before given RenderNet to render the albedo map. This is equivalent to assigning a texture value to the corresponding voxel in the binary shape voxel grid. We also add another output branch of 2D convolutions to RenderNet to render the normal map. The albedo map and the normal map produced by RenderNet are then combined to create shaded renderings of faces as described in Section 3.3. See Section 2.3 in the supplementary document for network architecture details.

4.2 Architecture comparison

In this section, we compare RenderNet with two baseline encoder-decoder architectures to render Phong-shaded images. Similar to RenderNet, the networks receive the 3D shape, pose, light position and light intensity as input. In contrast to RenderNet, the 3D shape given to the alternative network is in the canonical pose, and the networks have to learn to transform the 3D input to the given pose. The first network follows the network architecture by Dosovitskiy et al. [16], which consists of a

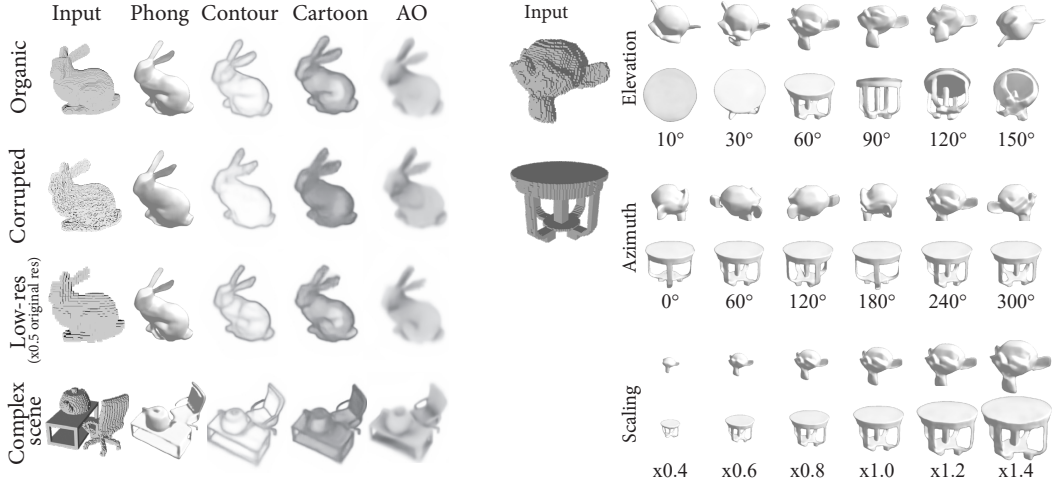


Figure 3: **Generalization.** Even with input from unseen categories or of low quality, RenderNet can still produce good results in different styles (left) and from different views (right).

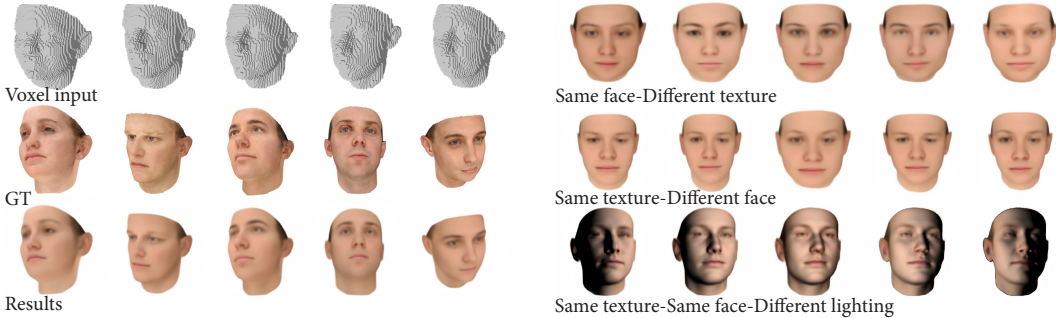


Figure 4: Rendering texture and manipulating rendering inputs. Best viewed in color.

series of fully-connected layers and up-convolution layers. The second network is similar but has a deeper decoder than the first one by adding residual blocks. For the 3D shape, we use an encoding network to map the input to a latent shape vector (refer to Section 2.2 in the supplementary document for details). We call these two networks EC and EC-Deep, respectively. These networks are trained directly on shaded images with a binary cross-entropy loss, using the chair category from ShapeNet. RenderNet, on the other hand, first renders the normal map, and combines this with the lighting input to create the shaded image using the shading equation in Section 3.3.

As shown in Figure 5, the alternative model (here we show the EC model) fails to produce important details of the objects and achieves lower PSNR score on the Phong-shaded chair dataset. More importantly, this architecture “remembers” the global structure of the objects and fails to generalize to objects of unseen category due to the use of the fully connected layers. In contrast, our model is better for rendering tasks as it generalizes well to different categories of shapes and scenes.

4.3 Shape reconstruction from images

Here we demonstrate that RenderNet can be used for single-image reconstruction. It achieves this goal via an iterative optimization that minimizes the following reconstruction loss:

$$\underset{z, \theta, \phi, \eta}{\text{minimize}} \quad \|I - f(z, \theta, \phi, \eta)\|^2 \quad (2)$$

where I is the observed image and f is our pre-trained RenderNet. z is the shape to reconstruct, θ and η are the pose and lighting parameters, and ϕ is the texture variable. In essence, this process maximizes the likelihood of observing the image I given the shape z .

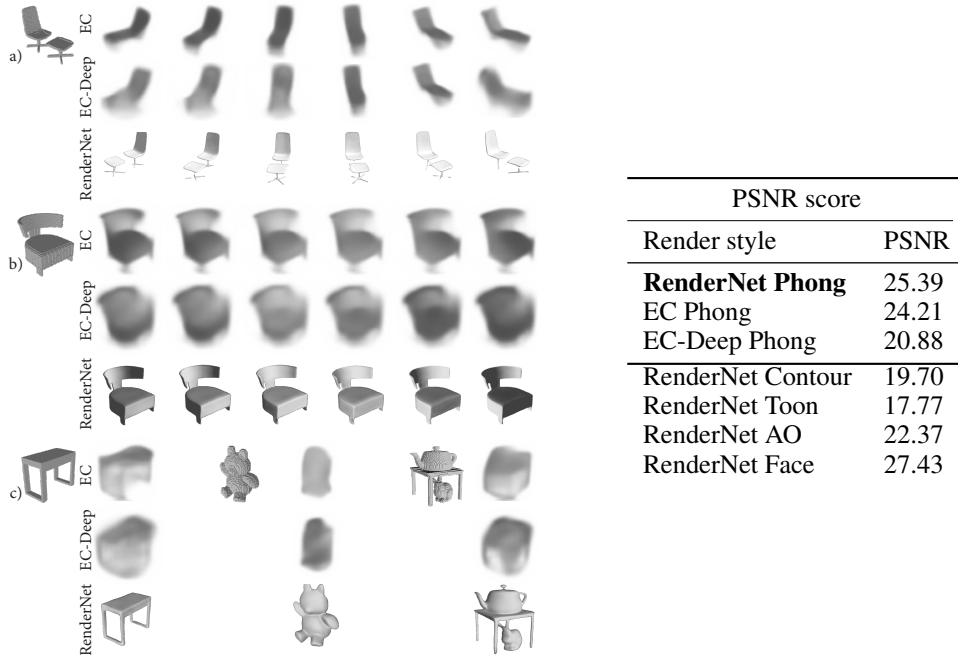


Figure 5: **Left:** Architecture comparison in different tasks: **a)** Novel-view synthesis, **b)** Relighting and **c)** Generalization. **Right:** PSNR score of different shaders, including the two alternative architectures.

However, directly minimizing this loss often leads to noisy, unstable results (shown in Figure 2 in the supplementary document). In order to improve the reconstruction, we use a shape prior for regularizing the process – a pre-trained 3D auto-encoder similar to the TL-embedding network [39] with 80000 shapes. Instead of optimizing z , we optimize its latent representation z' :

$$\underset{z', \theta, \phi', \eta}{\text{minimize}} \quad \|I - f(g(z'), \theta, h(\phi'), \eta)\|^2 \quad (3)$$

where g is the decoder of the 3D auto-encoder. It regularizes the reconstructed shape $g(z')$ by using the prior shape knowledge (weights in the decoder) for shape generation. Similarly, we use the decoder h that was trained with RenderNet for the texture rendering task in Section 4.1 to regularize the texture variable ϕ' . This corresponds to MAP estimation, where the prior term is the shape decoder and the likelihood term is given by RenderNet. Note that it is straightforward to extend this method to the multi-view reconstruction task by summing over multiple per-image losses with shared shape and appearance.

We compare RenderNet with DC-IGN by Kulkarni et al. [29] in Figure 6. DC-IGN learns to decompose images into a graphics code Z , which is a disentangled representation containing a set of latent variables for shape, pose and lighting, allowing them to manipulate these properties to generate novel views or perform image relighting. In contrast to their work, we explicitly reconstruct the 3D geometry, pose, lighting and texture, which greatly improves tasks such as out-of-plane rotation, and allows us to do re-texturing. We also generate results with much higher resolution (512×512) compared to DC-IGN (150×150). Our results show that having an explicit reconstruction not only creates sharper images with higher level of details in the task of novel-view prediction, but also gives us more control in the relighting task such as light color, brightness, or light position (here we manipulate the elevation and azimuth of the light position), and especially, the re-texturing task.

For the face dataset, we report the Intersection-over-Union (IOU) between the ground truth and reconstructed voxel grid of 42.99 ± 0.64 for 95% confidence interval. We also perform the same experiment for the chair dataset – refer to Section 1 in the supplementary material for implementation details and additional results.

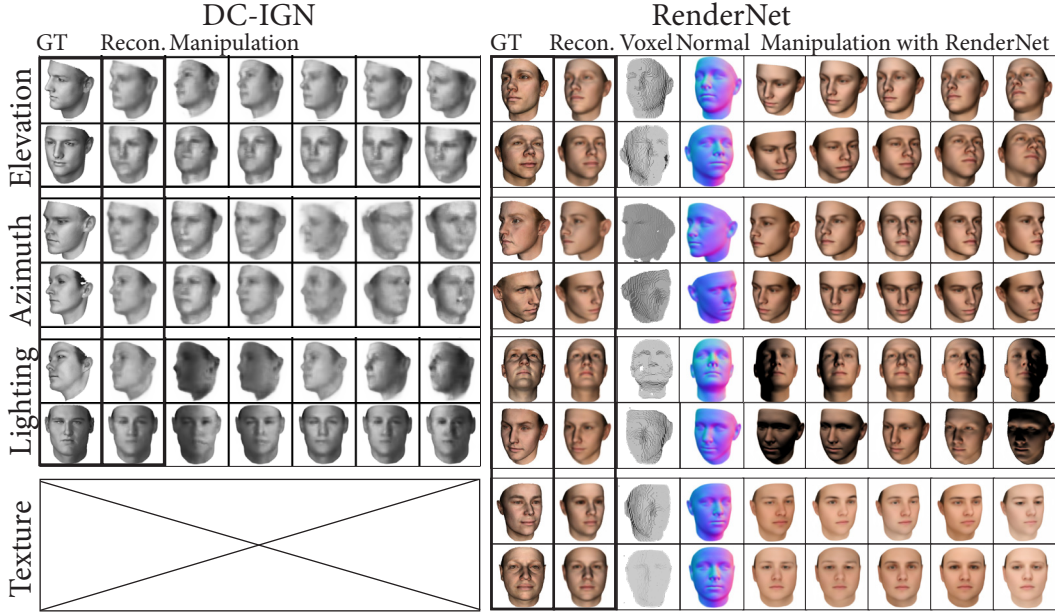


Figure 6: **Image-based reconstruction.** We show both the reconstructed images and normal maps from a single image. The cross indicates a factor not learnt by the network. Note: for the re-texturing task, we only show the albedo to visualize the change in texture more clearly. Best viewed in color.

5 Discussion and conclusion

In this paper, we presented RenderNet, a convolutional differentiable rendering network that can be trained end-to-end with a pixel-space regression loss. Despite the simplicity in the design of the network architecture and the projection unit, our experiments demonstrate that RenderNet successfully performs rendering and inverse rendering. Moreover, as shown in Section 4.1, there is the potential to combine different shaders in one network that shares the same 3D convolutions and projection unit, instead of training different networks for different shaders. This opens up room for improvement and exploration, such as extending RenderNet to work with unlabelled data, using other losses like adversarial losses or perceptual losses, or combining RenderNet with other architectures, such as U-Net or a multi-scale architecture where the projection unit is used at different resolutions. Another interesting possibility is to combine RenderNet with a style-transfer loss for stylization of 3D renderings.

The real world is three-dimensional, yet the majority of current image synthesis CNNs, such as GAN [17] or DC-IGN [29], only operates in 2D feature space and makes almost no assumptions about the 3D world. Although these methods yield impressive results, we believe that having a more geometrically grounded approach can greatly improve the performance and the fidelity of the generated images, especially for tasks such as novel-view synthesis, or more fine-grained editing tasks such as texture editing. For example, instead of having a GAN generate images from a noise vector via 2D convolutions, a GAN using RenderNet could first generate a 3D shape, which is then rendered to create the final image. We hope that RenderNet can bring more attention to the computer graphics literature, especially geometry-grounded approaches, to inspire future developments in computer vision.

Acknowledgments

We thank Christian Richardt for helpful discussions. We thank Lucas Theis for helpful discussions and feedback on the manuscript. This work was supported in part by the European Union’s Horizon 2020 research and innovation programme under the Marie Skłodowska-Curie grant agreement No 665992, the UK’s EPSRC Centre for Doctoral Training in Digital Entertainment (CDE), EP/L016540/1, and CAMERA, the RCUK Centre for the Analysis of Motion, Entertainment Research and Applications, EP/M023281/1. We also received GPU support from Lambda Labs.

References

- [1] Danilo Jimenez Rezende, S. M. Ali Eslami, Shakir Mohamed, Peter Battaglia, Max Jaderberg, and Nicolas Heess. Unsupervised learning of 3d structure from images. In *NIPS*, pages 4996–5004. 2016.
- [2] Matthew M. Loper and Michael J. Black. OpenDR: An approximate differentiable renderer. In *ECCV*, pages 154–169. 2014.
- [3] Hiroharu Kato, Yoshitaka Ushiku, and Tatsuya Harada. Neural 3d mesh renderer. In *IEEE CVPR*, 2018.
- [4] Xinchun Yan, Jimei Yang, Ersin Yumer, Yijie Guo, and Honglak Lee. Perspective transformer nets: Learning single-view 3d object reconstruction without 3d supervision. In *NIPS*, pages 1696–1704. 2016.
- [5] Rui Zhu, Hamed Kiani Galoogahi, Chaoyang Wang, and Simon Lucey. Rethinking reprojection: Closing the loop for pose-aware shape reconstruction from a single image. In *IEEE CVPR*, pages 57–65, 2017.
- [6] Jiajun Wu, Yifan Wang, Tianfan Xue, Xingyuan Sun, William T Freeman, and Joshua B Tenenbaum. MarrNet: 3D Shape Reconstruction via 2.5D Sketches. In *NIPS*, 2017.
- [7] Shubham Tulsiani, Tinghui Zhou, Alexei A. Efros, and Jitendra Malik. Multi-view supervision for single-view reconstruction via differentiable ray consistency. In *IEEE CVPR*, pages 209–217, 2017.
- [8] Paul Henderson and Vittorio Ferrari. Learning to generate and reconstruct 3d meshes with only 2d supervision. In *British Machine Vision Conference (BMVC)*, 2018.
- [9] Kyle Genova, Forrester Cole, Aaron Maschinot, Aaron Sarna, Daniel Vlasic, and William T. Freeman. Unsupervised training for 3d morphable model regression. In *The IEEE Conference on Computer Vision and Pattern Recognition (CVPR)*, June 2018.
- [10] Abhijit Kundu, Yin Li, and James M. Rehg. 3d-rcnn: Instance-level 3d object reconstruction via render-and-compare. In *CVPR*, 2018.
- [11] E. Richardson, M. Sela, R. Or-El, and R. Kimmel. Learning detailed face reconstruction from a single image. In *2017 IEEE Conference on Computer Vision and Pattern Recognition (CVPR)*, pages 5553–5562, July 2017. doi: 10.1109/CVPR.2017.589.
- [12] JunYoung Gwak, Christopher B Choy, Manmohan Chandraker, Animesh Garg, and Silvio Savarese. Weakly supervised 3d reconstruction with adversarial constraint. In *3D Vision (3DV), 2017 Fifth International Conference on 3D Vision*, 2017.
- [13] Min Lin, Qiang Chen, and Shuicheng Yan. Network in network. In *ICLR*, 2014.
- [14] Gao Huang, Zhuang Liu, Laurens van der Maaten, and Kilian Q Weinberger. Densely connected convolutional networks. In *IEEE CVPR*, pages 2261–2269, 2017.
- [15] O. Ronneberger, P. Fischer, and T. Brox. U-net: Convolutional networks for biomedical image segmentation. In *Medical Image Computing and Computer-Assisted Intervention (MICCAI)*, volume 9351, pages 234–241, 2015.
- [16] Alexey Dosovitskiy, Jost Tobias Springenberg, Maxim Tatarchenko, and Thomas Brox. Learning to generate chairs, tables and cars with convolutional networks. 39(4):692–705, 2017.
- [17] Ian Goodfellow, Jean Pouget-Abadie, Mehdi Mirza, Bing Xu, David Warde-Farley, Sherjil Ozair, Aaron Courville, and Yoshua Bengio. Generative adversarial nets. In Z. Ghahramani, M. Welling, C. Cortes, N. D. Lawrence, and K. Q. Weinberger, editors, *Advances in Neural Information Processing Systems 27*, pages 2672–2680. Curran Associates, Inc., 2014.
- [18] Qifeng Chen and Vladlen Koltun. Photographic image synthesis with cascaded refinement networks. In *IEEE ICCV*, pages 1520–1529, 2017.
- [19] Oliver Nalbach, Elena Arabadzhiyska, Dushyant Mehta, Hans-Peter Seidel, and Tobias Ritschel. Deep shading: Convolutional neural networks for screen-space shading. *Computer Graphics Forum (Proc. EGSR)*, 36(4):65–78, 2017.
- [20] Jonathan T Barron and Jitendra Malik. Shape, illumination, and reflectance from shading. *TPAMI*, 2015.
- [21] Tatsunori Taniai and Takanori Maehara. Neural inverse rendering for general reflectance photometric stereo. In *ICML*, volume 80 of *JMLR Workshop and Conference Proceedings*, pages 4864–4873. JMLR.org, 2018.

- [22] Maxim Tatarchenko, Alexey Dosovitskiy, and Thomas Brox. Octree generating networks: Efficient convolutional architectures for high-resolution 3d outputs. In *IEEE ICCV*, pages 2107–2115, 2017.
- [23] Peng-Shuai Wang, Yang Liu, Yu-Xiao Guo, Chun-Yu Sun, and Xin Tong. O-cnn: Octree-based convolutional neural networks for 3d shape analysis. *ACM TOG (Siggraph)*, 36(4):72:1–72:11, 2017.
- [24] Bui Tuong Phong. Illumination for computer generated pictures. *Commun. ACM*, 18(6):311–317, 1975.
- [25] Doug DeCarlo, Adam Finkelstein, Szymon Rusinkiewicz, and Anthony Santella. Suggestive contours for conveying shape. *ACM TOG (Siggraph)*, 22(3):848–855, July 2003.
- [26] Holger Winnemöller, Sven C. Olsen, and Bruce Gooch. Real-time video abstraction. *ACM TOG (Siggraph)*, 25(3):1221–1226, 2006.
- [27] Gavin Miller. Efficient algorithms for local and global accessibility shading. In *Proc. ACM SIGGRAPH*, pages 319–326, 1994.
- [28] Phillip Isola, Jun-Yan Zhu, Tinghui Zhou, and Alexei A. Efros. Image-to-image translation with conditional adversarial networks. In *IEEE CVPR*, pages 5967–5976, 2017.
- [29] Tejas D Kulkarni, William F. Whitney, Pushmeet Kohli, and Josh Tenenbaum. Deep convolutional inverse graphics network. In *NIPS*, pages 2539–2547, 2015.
- [30] Eunbyung Park, Jimei Yang, Ersin Yumer, Duygu Ceylan, and Alexander C. Berg. Transformation-grounded image generation network for novel 3d view synthesis. In *IEEE CVPR*, pages 702–711, 2017.
- [31] K. Rematas, C. H. Nguyen, T. Ritschel, M. Fritz, and T. Tuytelaars. Novel views of objects from a single image. *IEEE Trans. Pattern Anal. Mach. Intell.*, 39(8):1576–1590, 2017.
- [32] Jimei Yang, Scott E Reed, Ming-Hsuan Yang, and Honglak Lee. Weakly-supervised disentangling with recurrent transformations for 3d view synthesis. In *NIPS*, pages 1099–1107. 2015.
- [33] Hao Su, Fan Wang, Li Yi, and Leonidas J. Guibas. 3d-assisted image feature synthesis for novel views of an object. *CoRR*, abs/1412.0003, 2014.
- [34] Berthold K. P. Horn. Determining lightness from an image. *Computer Graphics and Image Processing*, 3(4):277–299, 1974.
- [35] Angel X. Chang, Thomas A. Funkhouser, Leonidas J. Guibas, Pat Hanrahan, Qi-Xing Huang, Zimo Li, Silvio Savarese, Manolis Savva, Shuran Song, Hao Su, Jianxiong Xiao, Li Yi, and Fisher Yu. Shapenet: An information-rich 3d model repository. *CoRR*, abs/1512.03012, 2015.
- [36] F. S. Nooruddin and G. Turk. Simplification and repair of polygonal models using volumetric techniques. *IEEE Trans. on Vis. and Comp. Graphics*, 9(2):191–205, 2003.
- [37] Pascal Paysan, Reinhard Knothe, Brian Amberg, Sami Romdhani, and Thomas Vetter. A 3d face model for pose and illumination invariant face recognition. In *Proceedings of the 2009 Sixth IEEE International Conference on Advanced Video and Signal Based Surveillance*, pages 296–301, 2009.
- [38] Diederik P. Kingma and Jimm Ba. Adam: A method for stochastic optimization. In *International Conference on Learning Representations (ICLR)*, 2015.
- [39] Rohit Girdhar, David F. Fouhey, Mikel Rodriguez, and Abhinav Gupta. Learning a predictable and generative vector representation for objects. In *ECCV*, pages 484–499, 2016.
- [40] Mathieu Aubry, Daniel Maturana, Alexei Efros, Bryan Russell, and Josef Sivic. Seeing 3d chairs: exemplar part-based 2d-3d alignment using a large dataset of cad models. In *CVPR*, 2014.
- [41] Shubham Tulsiani, Alexei A. Efros, and Jitendra Malik. Multi-view consistency as supervisory signal for learning shape and pose prediction. In *Computer Vision and Pattern Recognition (CVPR)*, 2018.
- [42] K. He, X. Zhang, S. Ren, and J. Sun. Delving deep into rectifiers: Surpassing human-level performance on imagenet classification. In *2015 IEEE International Conference on Computer Vision (ICCV)*, pages 1026–1034, Dec 2015.

Appendices

In this document, we provide more details for the image-based reconstruction task, and additional results for the chair dataset (Section A). We also provide more details for different network architectures (Section B). In Section C, we comment on the current limitations of RenderNet.

A Image-based reconstruction

A.1 Details on the optimization process

We optimize for the loss function:

$$\underset{z', \theta, \phi', \eta}{\text{minimize}} \quad \|I - f(g(z'), \theta, h(\phi'), \eta)\|^2 \quad (4)$$

where I is the observed image, z' is a latent vector representation of the 3D shape, g is the decoder of an autoencoder used to learn prior information about shapes (See Section A.3), θ is the pose parameter, η is the lighting parameter, ϕ' is the texture vector and h is the texture decoder. z' is a 200-dimensional vector in this experiment.

For the pose parameter θ , since we only observe faces from the frontal hemisphere, we subdivide the pose space of [0–180] degrees for azimuth, [0–180] degrees for elevation into a grid and use the grid points for initialization. The grid is later further subdivided around current best pose parameters. To avoid local minima, we initialize multiples of $(z'_i, \theta_i, \phi'_i, \eta_i)$ ($i \in \{1, 2, \dots, 5\}$ in our experiment) and use gradient descent for optimizing all of the variables. We re-initialise the parameters with the current best ones after every 200 steps, and continue with the optimization until convergence, which takes around 1800 steps.

A.2 Chair reconstruction from a single image

We optimize for the loss function:

$$\underset{z, \theta}{\text{minimize}} \quad \alpha \|I - f(g(z'), \theta)\|^2 + \beta (z - \mu)^T \Sigma^{-1} (z - \mu) \quad (5)$$

where I is the observed image, z' is a latent vector representation of the 3D shape, g is the decoder of an autoencoder used to learn prior information about shapes, θ is the pose parameter, μ and Σ are the mean and covariance of z' estimated from the training set respectively, and α and β are the weights of the loss terms (we use $\alpha = 5$, $\beta = 1$). z' is a 250-dimensional vector in this experiment. We also compare with DC-IGN [29], however, we could not download the same dataset [40] that was used for DC-IGN due to broken download links. Therefore, we use the chair category from ShapeNet, which is very similar and greatly overlaps with the dataset used in DC-IGN, as a substitute in this experiment. We use these chair models to create greyscale shaded images used as inputs for the reconstruction task.

We adopt the same optimisation strategy as with the face reconstruction (grid subdivision and gradient descent for the pose and shape vector). The optimisation converges after 2000 steps. The results are shown in Figure 7. Reconstructing chairs is a much more challenging task than reconstructing faces, due to the larger search space for the pose parameter ([0–360] for azimuth, [0–180] for elevation), as well as the larger variance in the geometry of different chairs, especially those containing very thin parts, that might not be fully captured by the shape prior. However, for a task as challenging as simultaneous shape and pose estimation, the results show great potential of our method, instead of using a feed-forward network similar to the work of Tulsiani et al. [41]. Further work is needed to improve the speed and performance of this method.

A.3 3D shape autoencoder for learning shape prior

We train an autoencoder to learn a prior of 3D shapes. The encoder is a series of 3D convolutions with channels {64, 128, 256, 512}, kernel sizes {5, 5, 2, 2}, and strides {2, 2, 2, 2} respectively. The fully-connected layer in the middle maps the output of the last convolution layer to a 200-dimensional vector. This is followed by a sigmoid activation function and another fully-connected layer that maps the 200-dimensional vector to a $(4 \cdot 4 \cdot 512)$ -dimensional vector. This vector is then reshaped to a tensor of size $4 \times 4 \times 512$ before being fed to a series of 3D up-convolutions with channels {256, 128, 64, 32, 1}, kernel sizes {4, 4, 4, 4, 4}, and strides {2, 2, 2, 2, 1}. Here we use ELU activation functions for all layers, apart from the last convolution layer in the encoder and decoder, which uses sigmoid functions.

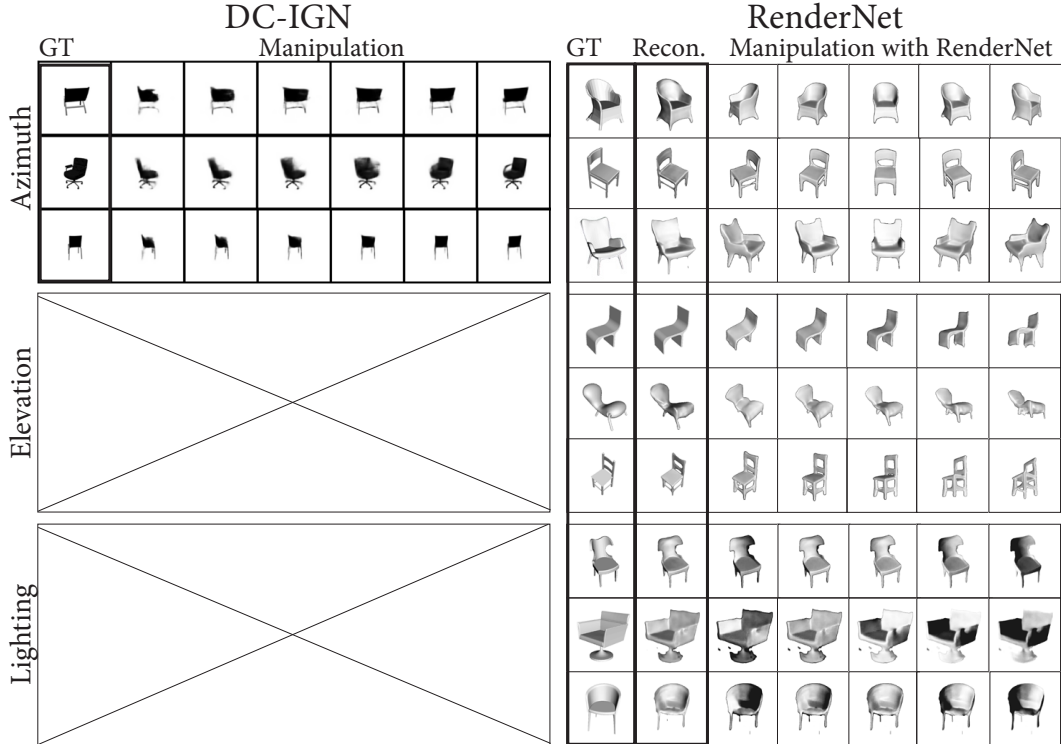


Figure 7: Reconstructing chairs from a single image, compared to DC-IGN [29]. The crosses indicate factors not learnt by the network. We were able to recover both the pose and shape of the chairs, which can be used to achieve sharper results in the task of novel-view synthesis, as well as enabling image relighting.

A.4 Reconstruction without prior

To show the importance of using the shape prior $g(z')$, here we compare the reconstruction results between those with the shape prior and those without, i.e., we directly optimize for the shape z without using the prior $g(z')$. Figure 8 shows that the reconstruction without using the shape prior fails to generate good results.

B Network Architecture

All of our layers use parametric Relu (PReLU) [42], apart from the last layer, which uses a sigmoid function. We also use dropouts with the probability of 0.5 during training after every convolution, except those used in the residual blocks.

Each 3D residual block consists of a $3 \times 3 \times 3$ 3D convolution, a PReLU activation function, and another $3 \times 3 \times 3$ 3D convolution. The input to the block is then added to the output of the second convolution (shortcut connection). Each 2D residual block is similar to the 3D one, but we replace 3D convolutions with 2D convolutions.

B.1 RenderNet

The 3D input encoder consists of an encoder made up of 3D convolutions with channels $\{8, 16, 16\}$, kernel sizes $\{5, 3, 3\}$, and strides $\{2, 2, 1\}$ respectively. We add ten 3D residual blocks, before feeding the result of the last block to the projection unit. The unit resizes the tensor from $W \times H \times 32 \times 16$ to $W \times H \times (32 \cdot 16)$ before feeding it to a 1×1 convolution with the same number of channels. This is followed by ten 2D residual blocks, a 4×4 convolution with $(32 \cdot 8)$ channels, and another five 2D residual blocks. To produce the final rendered image, we use a series of 2D convolutions with channels $\{32 \cdot 4, 32 \cdot 2, 32, 16, 3$ (or 1 for greyscale image)}, kernel sizes $\{4, 4, 4, 4, 4\}$ and strides $\{1, 2, 2, 2, 1\}$, respectively. To generate other modalities of the output (for example, in Section 4.1 where we render both the albedo map and normal map), we simply create another branch of 2D convolutions layers starting at the first strided up-convolution layer, and train it jointly with the rest of the network. This allows different modalities to share high-level information, such as object visibility, and

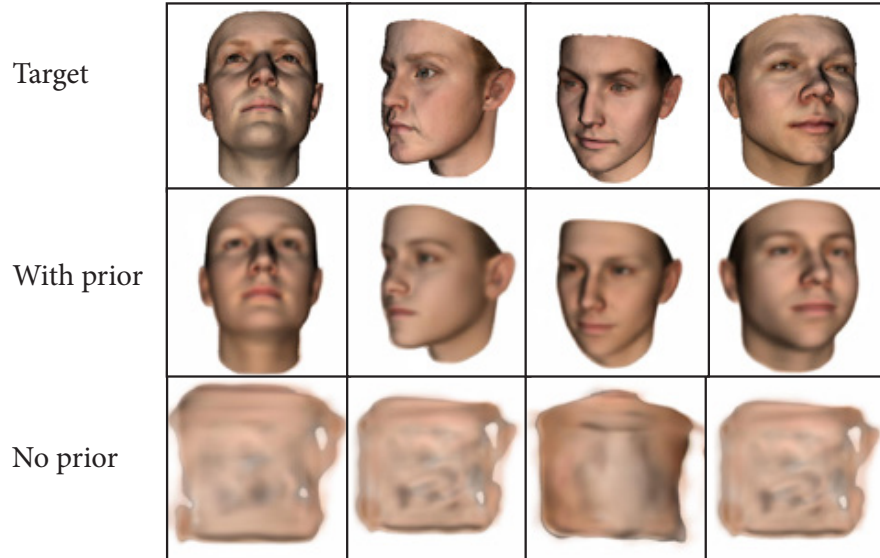


Figure 8: Comparison between the reconstruction results with/without prior.

only differ in the pixel appearance (shading). This shows the potential to combine training different shading styles into training one model that shares high-level information and separates low-level convolution layers for different shading styles.

B.2 Alternative architecture

Here we describe the architecture of the two alternative models EC and EC-deep that are used to compare against RenderNet (see Section 4.2 in the main paper).

The 3D input encoder consists of an encoder made up of 3D convolutions with channels $\{64, 128, 256, 512\}$, kernel sizes $\{4, 4, 4, 4\}$, and strides $\{2, 2, 2, 2\}$ respectively. All of these convolutions use parametric ReLU. This is followed by a fully-connected layer to map the tensors to a 200-dimensional vector and a sigmoid activation function.

For EC, we directly concatenate the lighting and pose parameters to the shape latent vector. For EC-deep, we feed each of them through a fully-connected layer to map each to a 512-dimensional vector. These two vectors are then concatenated to the shape latent vector. The final concatenated vector is then fed through 2 fully-connected layers to map to a 1024-dimensional vector, and another fully-connected layer to map to a $(8 \cdot 8 \cdot 512)$ -dimensional vector. The output of this layer is reshaped into a tensor of size $8 \times 8 \times 512$ before being fed to the decoder.

For EC, the decoder consists of 2D convolutions with 4×4 kernels with channels $\{512, 512, 256, 256, 128, 128, 64, 64, 32, 32, 16, 1\}$ and strides $\{2, 1, 2, 1, 2, 1, 2, 1, 2, 1, 2, 1\}$. For EC-deep, we replace each non-strided convolution in EC with two 2D residual blocks.

B.3 Texture decoder

The texture decoder consists of a fully-connected layer to map the 199-dimensional vector input to a vector of size $(32 \cdot 32 \cdot 32 \cdot 4)$, which is then reshaped into a tensor of size $32 \times 32 \times 32 \times 4$. This is followed by a series of 3D convolutions with channels $\{4, 8, 4\}$, kernel sizes $\{4, 4, 4\}$, and strides $\{1, 2, 1\}$ respectively. The output is a tensor of size $64 \times 64 \times 64 \times 4$.

C Limitations

RenderNet was trained using mean squared error loss (or binary cross-entropy loss for greyscale images), which tends to create blurry results. The effect is more obvious in certain shaders, such as the Ambient Occlusion. This can potentially be solved by adding an adversarial loss, but we consider this to be future work.

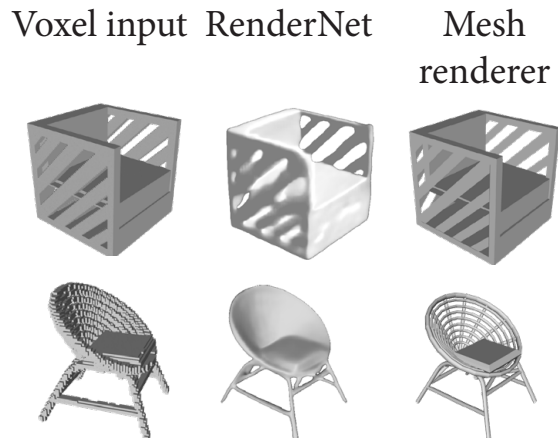


Figure 9: Failure cases.

Another potential limitation of our method is the input voxel grid resolution. We mitigate this limitation by training RenderNet on smaller, cropped voxel grids and running inference on larger voxel grids. This is made possible by the fully convolutional design of our architecture. Note that the output size is not limited. In the future, we could leverage data structures such as octrees or different data formats such as unstructured point clouds to further improve the scalability of our model.

As shown in Figure 9, RenderNet has a tendency to over-smooth sharp diagonal shapes. RenderNet also fails to render extremely thin features, which can easily be handled with the mesh renderer. However, this can be considered to be the limitation of the voxelizing tool, as the input voxel grid fails to capture very thin features, and not of RenderNet itself.

References

- [1] Danilo Jimenez Rezende, S. M. Ali Eslami, Shakir Mohamed, Peter Battaglia, Max Jaderberg, and Nicolas Heess. Unsupervised learning of 3d structure from images. In *NIPS*, pages 4996–5004. 2016.
- [2] Matthew M. Loper and Michael J. Black. OpenDR: An approximate differentiable renderer. In *ECCV*, pages 154–169. 2014.
- [3] Hiroharu Kato, Yoshitaka Ushiku, and Tatsuya Harada. Neural 3d mesh renderer. In *IEEE CVPR*, 2018.
- [4] Xinchen Yan, Jimei Yang, Ersin Yumer, Yijie Guo, and Honglak Lee. Perspective transformer nets: Learning single-view 3d object reconstruction without 3d supervision. In *NIPS*, pages 1696–1704. 2016.
- [5] Rui Zhu, Hamed Kiani Galoogahi, Chaoyang Wang, and Simon Lucey. Rethinking reprojection: Closing the loop for pose-aware shape reconstruction from a single image. In *IEEE CVPR*, pages 57–65, 2017.
- [6] Jiajun Wu, Yifan Wang, Tianfan Xue, Xingyuan Sun, William T Freeman, and Joshua B Tenenbaum. MarrNet: 3D Shape Reconstruction via 2.5D Sketches. In *NIPS*, 2017.
- [7] Shubham Tulsiani, Tinghui Zhou, Alexei A. Efros, and Jitendra Malik. Multi-view supervision for single-view reconstruction via differentiable ray consistency. In *IEEE CVPR*, pages 209–217, 2017.
- [8] Paul Henderson and Vittorio Ferrari. Learning to generate and reconstruct 3d meshes with only 2d supervision. In *British Machine Vision Conference (BMVC)*, 2018.
- [9] Kyle Genova, Forrester Cole, Aaron Maschinot, Aaron Sarna, Daniel Vlasic, and William T. Freeman. Unsupervised training for 3d morphable model regression. In *The IEEE Conference on Computer Vision and Pattern Recognition (CVPR)*, June 2018.
- [10] Abhijit Kundu, Yin Li, and James M. Rehg. 3d-rnn: Instance-level 3d object reconstruction via render-and-compare. In *CVPR*, 2018.
- [11] E. Richardson, M. Sela, R. Or-El, and R. Kimmel. Learning detailed face reconstruction from a single image. In *2017 IEEE Conference on Computer Vision and Pattern Recognition (CVPR)*, pages 5553–5562, July 2017. doi: 10.1109/CVPR.2017.589.

- [12] JunYoung Gwak, Christopher B Choy, Manmohan Chandraker, Animesh Garg, and Silvio Savarese. Weakly supervised 3d reconstruction with adversarial constraint. In *3D Vision (3DV), 2017 Fifth International Conference on 3D Vision*, 2017.
- [13] Min Lin, Qiang Chen, and Shuicheng Yan. Network in network. In *ICLR*, 2014.
- [14] Gao Huang, Zhuang Liu, Laurens van der Maaten, and Kilian Q Weinberger. Densely connected convolutional networks. In *IEEE CVPR*, pages 2261–2269, 2017.
- [15] O. Ronneberger, P.Fischer, and T. Brox. U-net: Convolutional networks for biomedical image segmentation. In *Medical Image Computing and Computer-Assisted Intervention (MICCAI)*, volume 9351, pages 234–241, 2015.
- [16] Alexey Dosovitskiy, Jost Tobias Springenberg, Maxim Tatarchenko, and Thomas Brox. Learning to generate chairs, tables and cars with convolutional networks. 39(4):692–705, 2017.
- [17] Ian Goodfellow, Jean Pouget-Abadie, Mehdi Mirza, Bing Xu, David Warde-Farley, Sherjil Ozair, Aaron Courville, and Yoshua Bengio. Generative adversarial nets. In Z. Ghahramani, M. Welling, C. Cortes, N. D. Lawrence, and K. Q. Weinberger, editors, *Advances in Neural Information Processing Systems 27*, pages 2672–2680. Curran Associates, Inc., 2014.
- [18] Qifeng Chen and Vladlen Koltun. Photographic image synthesis with cascaded refinement networks. In *IEEE ICCV*, pages 1520–1529, 2017.
- [19] Oliver Nalbach, Elena Arabadzhiyska, Dushyant Mehta, Hans-Peter Seidel, and Tobias Ritschel. Deep shading: Convolutional neural networks for screen-space shading. *Computer Graphics Forum (Proc. EGSR)*, 36(4):65–78, 2017.
- [20] Jonathan T Barron and Jitendra Malik. Shape, illumination, and reflectance from shading. *TPAMI*, 2015.
- [21] Tatsunori Tani and Takahiro Maehara. Neural inverse rendering for general reflectance photometric stereo. In *ICML*, volume 80 of *JMLR Workshop and Conference Proceedings*, pages 4864–4873. JMLR.org, 2018.
- [22] Maxim Tatarchenko, Alexey Dosovitskiy, and Thomas Brox. Octree generating networks: Efficient convolutional architectures for high-resolution 3d outputs. In *IEEE ICCV*, pages 2107–2115, 2017.
- [23] Peng-Shuai Wang, Yang Liu, Yu-Xiao Guo, Chun-Yu Sun, and Xin Tong. O-cnn: Octree-based convolutional neural networks for 3d shape analysis. *ACM TOG (Siggraph)*, 36(4):72:1–72:11, 2017.
- [24] Bui Tuong Phong. Illumination for computer generated pictures. *Commun. ACM*, 18(6):311–317, 1975.
- [25] Doug DeCarlo, Adam Finkelstein, Szymon Rusinkiewicz, and Anthony Santella. Suggestive contours for conveying shape. *ACM TOG (Siggraph)*, 22(3):848–855, July 2003.
- [26] Holger Winnemöller, Sven C. Olsen, and Bruce Gooch. Real-time video abstraction. *ACM TOG (Siggraph)*, 25(3):1221–1226, 2006.
- [27] Gavin Miller. Efficient algorithms for local and global accessibility shading. In *Proc. ACM SIGGRAPH*, pages 319–326, 1994.
- [28] Phillip Isola, Jun-Yan Zhu, Tinghui Zhou, and Alexei A. Efros. Image-to-image translation with conditional adversarial networks. In *IEEE CVPR*, pages 5967–5976, 2017.
- [29] Tejas D Kulkarni, William F. Whitney, Pushmeet Kohli, and Josh Tenenbaum. Deep convolutional inverse graphics network. In *NIPS*, pages 2539–2547, 2015.
- [30] Eunbyung Park, Jimei Yang, Ersin Yumer, Duygu Ceylan, and Alexander C. Berg. Transformation-grounded image generation network for novel 3d view synthesis. In *IEEE CVPR*, pages 702–711, 2017.
- [31] K. Rematas, C. H. Nguyen, T. Ritschel, M. Fritz, and T. Tuytelaars. Novel views of objects from a single image. *IEEE Trans. Pattern Anal. Mach. Intell.*, 39(8):1576–1590, 2017.
- [32] Jimei Yang, Scott E Reed, Ming-Hsuan Yang, and Honglak Lee. Weakly-supervised disentangling with recurrent transformations for 3d view synthesis. In *NIPS*, pages 1099–1107. 2015.
- [33] Hao Su, Fan Wang, Li Yi, and Leonidas J. Guibas. 3d-assisted image feature synthesis for novel views of an object. *CoRR*, abs/1412.0003, 2014.
- [34] Berthold K. P. Horn. Determining lightness from an image. *Computer Graphics and Image Processing*, 3(4):277–299, 1974.

- [35] Angel X. Chang, Thomas A. Funkhouser, Leonidas J. Guibas, Pat Hanrahan, Qi-Xing Huang, Zimo Li, Silvio Savarese, Manolis Savva, Shuran Song, Hao Su, Jianxiong Xiao, Li Yi, and Fisher Yu. Shapenet: An information-rich 3d model repository. *CoRR*, abs/1512.03012, 2015.
- [36] F. S. Nooruddin and G. Turk. Simplification and repair of polygonal models using volumetric techniques. *IEEE Trans. on Vis. and Comp. Graphics*, 9(2):191–205, 2003.
- [37] Pascal Paysan, Reinhard Knothe, Brian Amberg, Sami Romdhani, and Thomas Vetter. A 3d face model for pose and illumination invariant face recognition. In *Proceedings of the 2009 Sixth IEEE International Conference on Advanced Video and Signal Based Surveillance*, pages 296–301, 2009.
- [38] Diederik P. Kingma and Jimm Ba. Adam: A method for stochastic optimization. In *International Conference on Learning Representations (ICLR)*, 2015.
- [39] Rohit Girdhar, David F. Fouhey, Mikel Rodriguez, and Abhinav Gupta. Learning a predictable and generative vector representation for objects. In *ECCV*, pages 484–499, 2016.
- [40] Mathieu Aubry, Daniel Maturana, Alexei Efros, Bryan Russell, and Josef Sivic. Seeing 3d chairs: exemplar part-based 2d-3d alignment using a large dataset of cad models. In *CVPR*, 2014.
- [41] Shubham Tulsiani, Alexei A. Efros, and Jitendra Malik. Multi-view consistency as supervisory signal for learning shape and pose prediction. In *Computer Vision and Pattern Recognition (CVPR)*, 2018.
- [42] K. He, X. Zhang, S. Ren, and J. Sun. Delving deep into rectifiers: Surpassing human-level performance on imagenet classification. In *2015 IEEE International Conference on Computer Vision (ICCV)*, pages 1026–1034, Dec 2015.